POLITECNICO DI TORINO
Repository ISTITUZIONALE

High sensitivity, low noise front-end for long range capacitive sensors for tagless indoor human localization

Original
High sensitivity, low noise front-end for long range capacitive sensors for tagless indoor human localization / Iqbal, J., Lazarescu, M.T., Arif, A., Lavagno, L.. - ELETTRONICO. - (2017), pp. 1-6. (IEEE International Forum on Research and Technologies for Society and Industry (RTSI2017) Modena, Italy 11-13 settembre 2017) [10.1109/RTSI.2017.8065966].

Availability:
This version is available at: 11583/2674970 since: 2020-10-22T14:55:52Z

Publisher:
IEEE

Published
DOI:10.1109/RTSI.2017.8065966

Terms of use:

This article is made available under terms and conditions as specified in the corresponding bibliographic description in the repository

Publisher copyright
IEEE postprint/Author's Accepted Manuscript

©2017 IEEE. Personal use of this material is permitted. Permission from IEEE must be obtained for all other uses, in any current or future media, including reprinting/republishing this material for advertising or promotional purposes, creating new collecting works, for resale or lists, or reuse of any copyrighted component of this work in other works.

(Article begins on next page)

10 October 2026

High sensitivity, low noise front-end for long range capacitive sensors for tagless indoor human localization

Javed Iqbal, Mihai Teodor Lazarescu, Arslan Arif and Luciano Lavagno
Department of Electronics and Telecommunications (DET)
Politecnico di Torino, Italy
email:{javed_iqbal; mihai.lazarescu; arslan.arif; luciano.lavagno}@polito.it

***Abstract*—Capacitive sensors are used in many applications due to their multiple advantages, but typically up to distances comparable to sensor dimensions. We present the design and the experimental results of a self-contained long range capacitive sensor front-end that is based on phase modulation and is suitable for indoor human localization. The changes in reactance due to the changes in the sensor capacitance modulate the phase of a carrier frequency, which is then demodulated using a XOR gate as quadrature detector. A phase modulated carrier is bot less susceptible to noise and easier to filter. The experimental results show a very good sensor sensitivity up to 150 cm for a 16 cm square sensor plate, very low noise and good measurement stability.**

Keywords: Long range capacitive sensor; low noise capacitive sensors; phase demodulation; tagless indoor human localization

I. Introduction

Indoor human detection, localization, tracking and activity monitoring are at the core of many health care monitoring and assisted living systems [1]. Many solutions have been proposed by the research and scientific community in this regard. Y. Zheng et al. present a vision-based indoor navigation system [2]. G. Lu et al. introduce an indoor localization system based on thermal imaging [3]. Both solutions are accurate and reliable, but require significant computational resources and energy, which also increase their cost. Moreover, image-based solutions often rise privacy concerns.

Other tagless indoor localization techniques include ultrasonic transceivers to localize indoor persons or objects [4], but extended exposure to ultrasounds can be harmful [5]. D. Yang et al. propose indoor human localization using pyroelectric infrared (PIR) sensors and an accessibility map [6]. A larger number of sensors were used since the PIR sensors have a narrow field of view [7] and they are also prone to errors due to ambient and heat sources, such as electric bulbs, sunshine, stoves, heaters.

The accuracy of the Wi-Fi-based indoor localization systems suffer from multipath interference [8]. Other radio frequency techniques are based on Bluetooth and RFID [4], [9], [10]. However, they require the person to carry a tag in order to be visible to the system, which can be both inconvenient and unreliable, since the persons may often forget to wear it.

Capacitive sensors are attractive for indoor person localization and activity monitoring due to their low cost and low power operation [11], [12], [13]. Capacitive sensors are also proposed for gesture recognition and human identification from a small group of people with distinct physiological traits [14], [15].

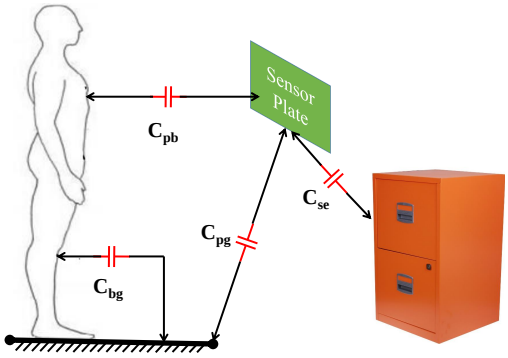

Fig. 1. Main capacitances that influence the overall capacitance of a load mode capacitive sensor

The total capacitance of a load mode capacitive sensor used for human localization is influenced by four main components: the capacitance between the sensor and the ground (C_{sg} **MTL: correct in Figure 1**), the capacitance between the human body and the ground (C_{bg}), the capacitance between the sensor and the environment (C_{se}) and capacitance between the sensor and the human body (C_{sb} **MTL: correct in Figure 1**). The latter depends on the distance, d, between the sensor and the human body, as shown in Fig. 1. Moreover, the ambient temperature and humidity also affect the value of the capacitance.

The sensitivity of the capacitive sensors is often limited by the environmental electromagnetic noise and the sensitivity of the interface. In fact, at distances beyond ten times the size of the sensor, the capacitance variation due to the presence of the human body can be below 0.01%, which is often hardly distinguishable from the noise. However, it should be noted that the noise affects mostly the measurement techniques (e.g., the measurement of the voltage across the capacitance) and much less the capacitance itself, which depends mostly on the geometry, and electric and dielectric properties of the sensor and the surrounding environment.

To extend the sensing distance of capacitive sensors, we

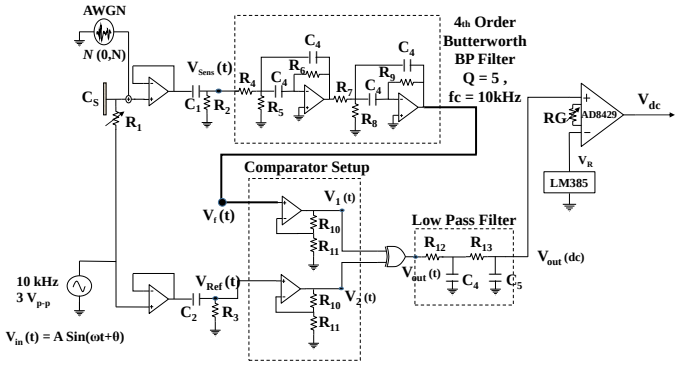

Fig. 2. Capacitive sensor front end interface

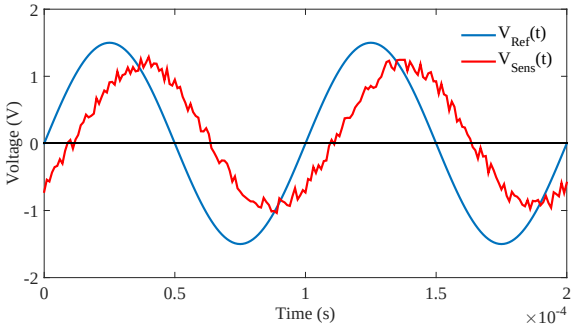

Fig. 3. Signals before filtering

present in this work the design and experimental results of a front end interface for loading mode capacitive sensors which can achieve high sensitivity, good stability and noise rejection.

The rest of the article is organized as follows. In Section II we discuss our main contributions. In Section III we present our methodology, i.e., the capacitive sensor front-end interface circuit design and the experimental setup. In Section IV we present and discuss the experiments and results. In Section V we discuss possible refinements and improvements of the method, and Section VI concludes the article.

II. Our Main Contributions

Capacitive sensing for ranges far longer than the dimension of the sensor presents multiple significant challenges. For instance, in a recent comprehensive survey on capacitive sensing methods only 12 works out of almost 200 address longer sensing range. Moreover, most of the sensing techniques require complex sensor topologies and tedious realization methods, which make them impractical for most applications, including the IoT.

In this work, we have designed, implemented and tested the front-end interface of a load mode capacitive sensor for indoor human localization. The interface measures the variable phase shift introduced by a lowpass filter that includes the capacitance of the transducer. The measurement technique is able to considerably reduce the environmental noise and provide a high sensitivity to capacitance variations with low cost components and low power consumption.

III. Methodology

A. Capacitive-sensor Front-end Interface Design

The front-end interface circuit of the capacitive sensor is shown in Fig. 2. It consists of two analog processing paths, both excited using the same signal source,

$$\mathrm{V_{in}(t)} = \mathrm{A}\sin(2\pi \mathrm{f t} + \theta), \tag{1}$$

with $\mathrm{A} = 3\,\mathrm{V_{pp}}$ and $\mathrm{f} = 10\,\mathrm{kHz}$.

On the upper path, the excitation signal enters a lowpass filter made of $\mathrm{R_1C_S}$, where $\mathrm{C_S}$ is the equivalent capacitance of the transducer of the sensor. The characteristics of the filter depend on the value of $\mathrm{C_S}$, whose value depends on the distance to the human body. Then the output of the $\mathrm{R_1C_S}$ filter is read using a high impedance voltage repeater, while on the lower path the excitation is sent directly to an identical reader circuit.

We model the noise captured by the sensor transducer, a $16\,\mathrm{cm}\times 16\,\mathrm{cm}$ metallic plate, as an additive white Gaussian noise generator (AWGN) at the input of the reader circuit on the top path. Hence, at the output of the top path reader circuit we have

$$\mathrm{V_{Sens}(t)} = \mathrm{B}\sin(2\pi \mathrm{f t} + \theta + \phi) + N(0, \mathrm{N}), \tag{2}$$

while at the output of the bottom path reader circuit we have

$$\mathrm{V_{Ref}(t)} = \mathrm{A}\sin(2\pi \mathrm{f t} + \theta), \tag{3}$$

where the amplitude is

$$\mathrm{B} = \frac{1}{\sqrt{1 + (2\pi \mathrm{f C_S R_1})^2}} \tag{4}$$

and the phase shift is

$$\phi = -\arctan(2\pi \mathrm{f C_S R_1}). \tag{5}$$

The high-pass filters that follow the reader circuits,$\mathrm{C_1R_2}$ and $\mathrm{C_2R_3}$, eliminate the very low frequency noise and DC offsets from the buffered signals.

The maximum phase shift sensitivity of an RC filter to variations of the filter capacitance is at the cutoff frequency. Hence, to improve the sensitivity of our filter we adjusted the value of $\mathrm{R_1}$ in order to tune the $\mathrm{R_1C_S}$ cutoff frequency to the excitation frequency, 10 kHz, for the value of $\mathrm{C_S}$ when nobody was present in sensor range.

At the cutoff frequency we have

$$\mathrm{B} = \frac{\mathrm{A}}{\sqrt{2}} \tag{6}$$

and

$$\phi = -\frac{\pi}{4}. \tag{7}$$

So, for the $\mathrm{R_1C_S}$ filter at cutoff we have

$$\mathrm{V_{Sens}(t)} = \frac{\mathrm{A}}{\sqrt{2}}\sin(2\pi \mathrm{f t} + \theta - \frac{\pi}{4}) + N(0, \mathrm{N}). \tag{8}$$

and the signals $\mathrm{V_{Ref}(t)}$ and $\mathrm{V_{Sens}(t)}$ are shown in Fig. 3.

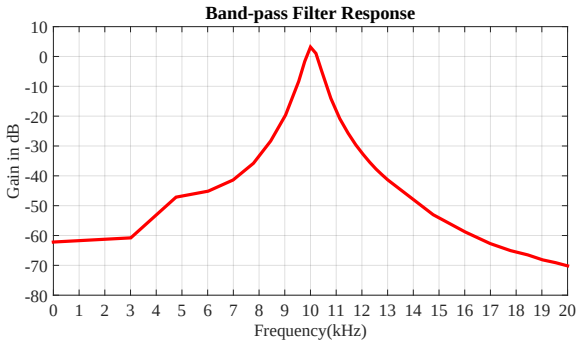

Fig. 4. Measured response of a 4th-order Butterworth bandpass filter with $f_C = 10$ kHz and $Q = 5$

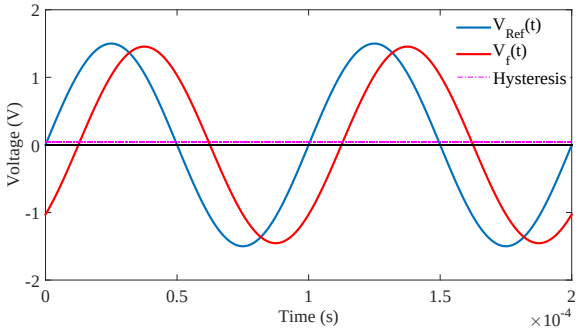

Fig. 5. Signals after filtering and hysteresis thresholds to prevent ringing at comparators output

$V_{Sens}(t)$ has a significant noise component that is captured by the plate of the capacitive transducer. Since we know the exact frequency of the excitation frequency, 10 kHz, we remove the noise using a narrow-band bandpass filter. The filter is placed only on the upper path of the sensor front-end shown in Fig. 2 and is implemented using a 4th order Butterworh bandpass filter with a quality factor $Q = 5$. The measured response of the filter is shown in Fig. 4. We can see that its pass-band gain is aboout 1.4, to compensate for the attenuation of the R_1C_S filter:

$$V_f(t) = 1.4\frac{A}{\sqrt{2}}\sin(2\pi ft + \theta - \frac{\pi}{4}). \tag{9}$$

The passband filter removes most of the noise from the signal, as shown in Fig. 5.

The signals of the two front-end paths, $V_{Ref}(t)$ and $V_f(t)$ (see Fig. 2), are then each passed through a hysteresis comparator to prepare them for the phase discriminator circuit that is implemented using a XOR logic gate. The comparator hysteresis is small, e.g., for a single 5 V supply operation the upper threshold voltage, V_{TH}, and lower threshold voltage, V_{TL}, are:

$$V_{TH} = V_{CC}\left(\frac{R_{11}}{R_{11}+R_{10}}\right), \tag{10}$$

$$V_{TL} = V_{EE}\left(\frac{R_{11}}{R_{11}+R_{10}}\right). \tag{11}$$

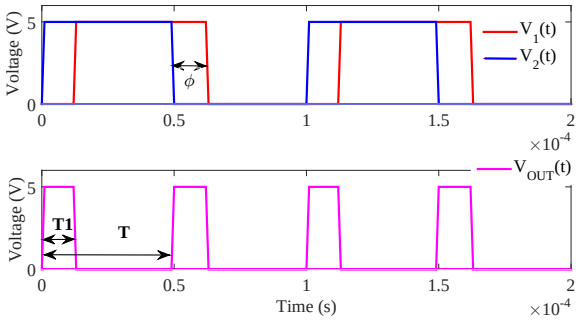

Fig. 6. Outputs of the comparators (upper plot) and the phase discriminator XOR gate (lower plot)

With $V_{CC} = 5$ V, $V_{EE} = 0$ V, $R_{10} = 100$ kΩ and $R_{11} = 1$ kΩ we get $V_{TH} \simeq 50$ mV and $V_{TL} = 0$ V.

The comparators generate $V_1(t)$ (on the upper path, from the R_1C_S sensor in Fig. 2) and $V_2(t)$. They are then passed through an XOR gate which generates $V_{out}(t)$, as shown in Fig. 6. The fundamental frequency of both $V_1(t)$ and $V_2(t)$ is 10 kHz, while the fundamental frequency of the output of the XOR gate, $V_{out}(t)$, is double, $f_o = 20$ kHz.

The non-zero average signal $V_{out}(t)$ can be represented as a Fourier series

$$V_{out}(t) = \frac{5T_1}{T} + \sum_{k=1}^{\infty}(A_k\cos(2k\pi f_o t) + B_k\sin(2k\pi f_o t)), \tag{12}$$

with

$$A_k = \frac{5}{k\pi}\left[\sin(\frac{2\pi kT_1}{T})\right], \tag{13}$$

$$B_k = \frac{5}{k\pi}\left[1 - \cos\left(\frac{2\pi kT_1}{T}\right)\right], \tag{14}$$

and T_1 depending directly on the variable phase shift introduced by the R_1C_S filter (see Fig. 2) based on the value of the overall capacitance of the sensor transducer, C_S, which depends on the position of the human body.

In order to obtain the DC component of the phase discriminator output, V_{out}, we use a 2nd-order lowpass filter which passes only the DC term,

$$V_{out}(dc) = \frac{5T_1}{T}. \tag{15}$$

Since $T_1 = f(\phi)$, when there is nobody in sensor range the cutoff frequency of the R_1C_S filter matches the excitation frequency of 10 kHz, so $\phi = -\frac{\pi}{4}$. Thus, we get $T_1 = \frac{T}{4}$, where $T = 50\,\mu$s.

Thus, with no person in sensor range we obtain a static output of 1.25 V. This offset is due to the minimum phase difference of $\frac{\pi}{4}$ between the two paths of the front-end. This minimum phase difference is needed in order to ensure that the XOR gate of the phase discriminator operates well within its normal operation parameters, i.e., we avoid very small phase differences (delays) between its input signals.

We remove most of this static offset using an adjustable voltage reference implemented using an LM385 voltage reference

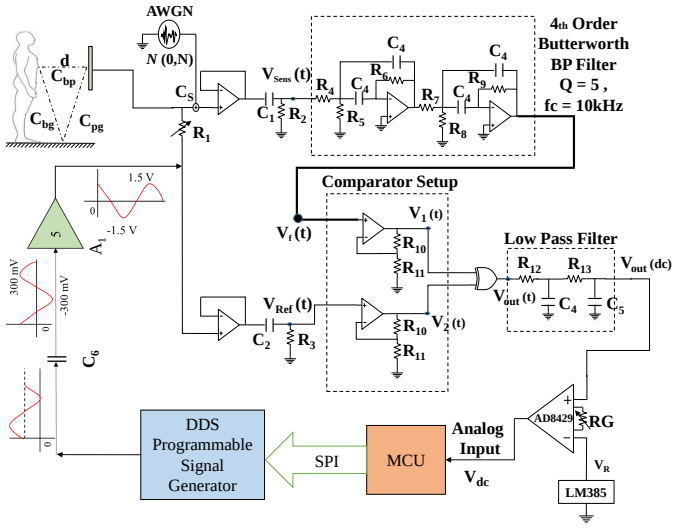

Fig. 7. Full circuit used for the experiments

and a precision instrumentation amplifier, AD8429, to obtain V_{dc} (see Fig. 2). We adjust R_G to set the instrumentation amplifier gain to $G = 80$. Hence,

$$V_{dc} = G\,(V_{out}(dc) - V_R). \tag{16}$$

(1)-(16) provide a closed form mathematical model of the front-end of our capacitive sensor. (15) and (16) show that the V_{dc} output depends on the $\frac{T_1}{T}$ ratio, of which T_1 is a function of the phase shift ϕ (5) introduced by the R_1C_S filter in Fig. 2, whose capacitance C_S depends on the distance to the human body. Thus, the output voltage V_{dc} changes with C_S, increasing as the person approaches the sensor from a minimum value when the person is outside the range of the sensor.

B. Experimental Setup

Fig. 7 shows the experimental setup that we used to perform the experiments. We programmed a direct digital synthesis (DDS) programmable waveform generator, AD9837, using the SPI interface of an ATmega328 microcontroller to generate a $10\,\mathrm{kHz}$ sine waveform. The DDS generates a $600\,\mathrm{mV_{pp}}$ signal with $300\,\mathrm{mV}$ DC offset, which is removed using C_6. A_1 amplifies the signal five times to provide the $3\,V_{pp}$ excitation signal. The demodulated output, V_{dc} (the output of the instrumentation amplifier), is measured directly by the built-in analog to digital converter (ADC) of the microcontroller.

As argued before, the value of the capacitance C_S is affected by many factors besides the position of the human body. So the measurements are not deterministic and we use multiple measurements over a certain period of time to study the statistical properties of the measured data.

IV. Experimental Results and Discussion

We measured the output voltage of the front-end, V_{dc}, while a person was standing in front of the sensor at a distance between $25\,\mathrm{cm}$ and $150\,\mathrm{cm}$, with steps of $25\,\mathrm{cm}$.

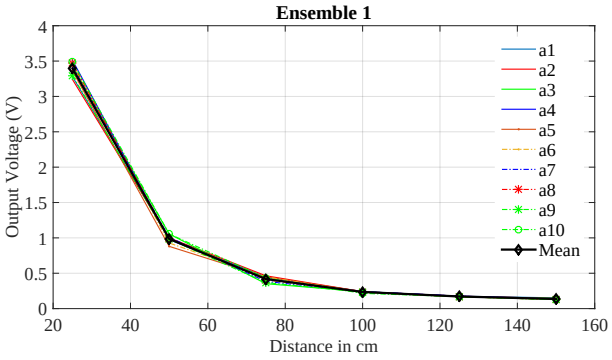

Fig. 8. Ensemble 1 of measurements

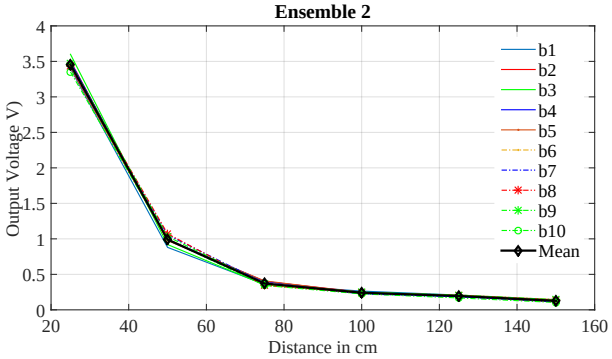

Fig. 9. Ensemble 2 of measurements

Due to random influences of C_S and V_{dc}, we have made multiple measurements for each position. Figs. 8-12 show the ensembles of measurements that we have made during a day in static room settings. In each ensemble are plotted ten measurement sets and their average. Each measurement set contains six measurements, one for each of the distances $25\,\mathrm{cm}$, $50\,\mathrm{cm}$, $75\,\mathrm{cm}$, $100\,\mathrm{cm}$, $125\,\mathrm{cm}$ and $150\,\mathrm{cm}$. Fig. 13 shows the averages of all five ensembles of measurements. We see that in static room conditions the sensor measurements show a good stability. Moreover, Fig. 14 shows the good sensitivity and resolution of the sensor even at long distances. The same can be seen from Table I, which shows the average output voltage vs. distance of the human body from the sensor,

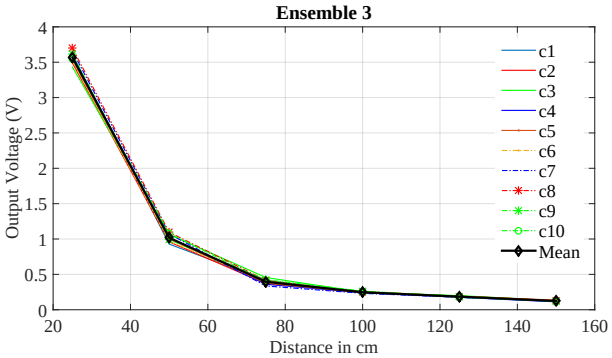

Fig. 10. Ensemble 3 of measurements

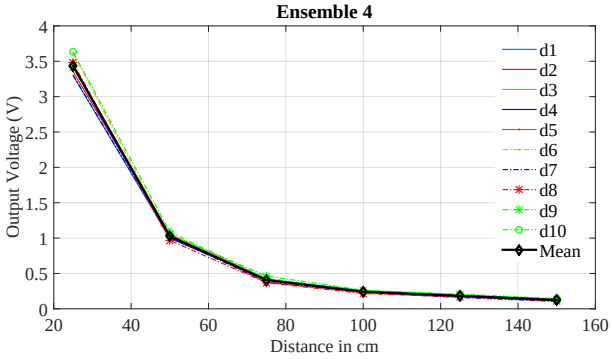

Fig. 11. Ensemble 4 of measurements

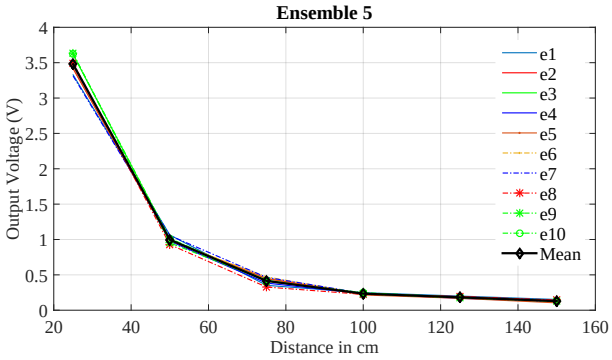

Fig. 12. Ensemble 5 of measurements

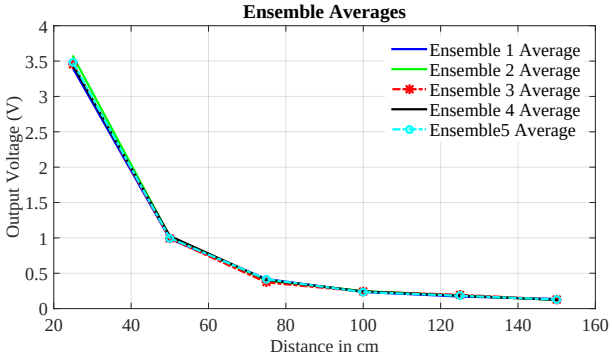

Fig. 13. Averages of the ensembles of measurements

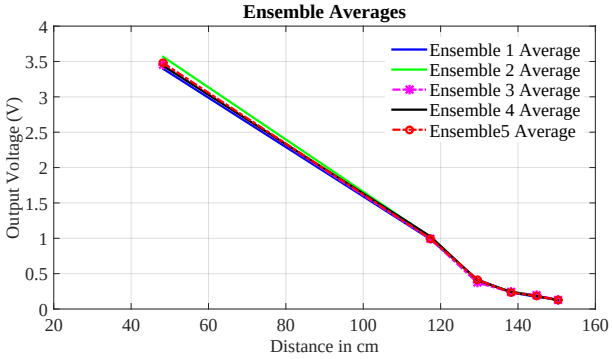

Fig. 14. Averages of the ensembles of measurements in logarithmic scale **MTL: the plot is in log scale, but the X axis is not.**

TABLE I
AVERAGE V_{dc} VS. DISTANCE FROM THE SENSOR AND OUTPUT VOLTAGE CHANGES IN 25 CM STEPS TOWARDS THE SENSOR

Distance (cm)	Average V_{dc} (V)	Voltage change per step (mV)
150	0.1360	—
125	0.1712	35
100	0.2352	64
75	0.4176	182
50	0.9864	568
25	3.3960	2400

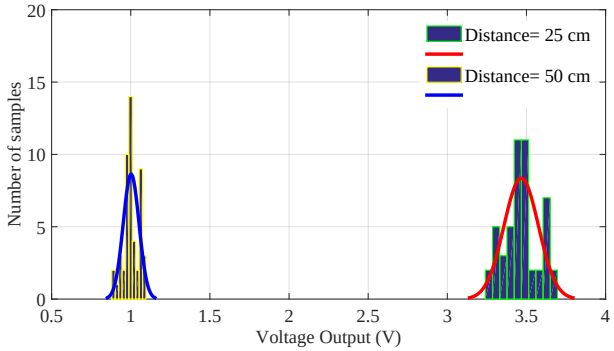

Fig. 15. Distribution of output voltage at distances of 25 cm and 50 cm

and the output voltage changes per step of 25 cm towards the sensor.

Fig. 15, 16 and 17 show the distributions of the output voltage vs. the distance of human body from the capacitive sensor. The dispersion is limited for all distances, which indicates a good sensor accuracy with sufficient signal-to-noise ratio. Ultimately, these translate in low localization errors.

V. FUTURE WORK AND IMPROVEMENTS

We intend to use multiple sensor nodes in a wireless sensor network (WSN) for indoor localization of a person. E.g., since our single sensor node can localize a person at distances up to 150 cm, with four sensor nodes on the four walls of a room we can use machine learning algorithms to localize a person inside a 3 m×3 m room.

We also intend to further optimize the power efficiency of the sensor using low power components and circuit solutions,

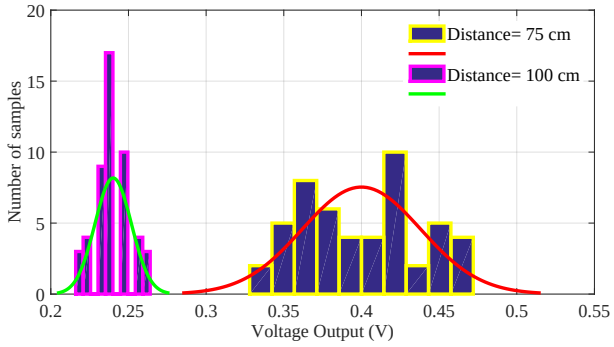

Fig. 16. Distribution of output voltage at distances of 75 cm and 100 cm

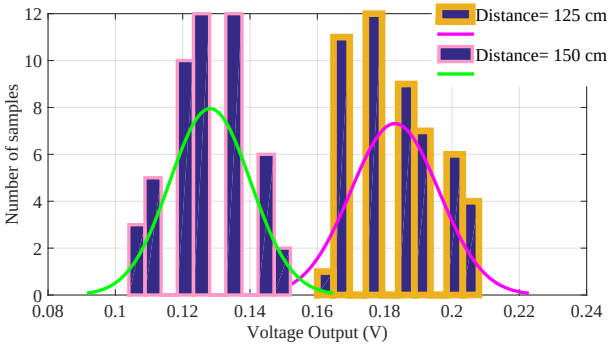

Fig. 17. Distribution of the output voltage at distances of 125 cm and 150 cm

and by duty cycling the operation of the sensor.

VI. Conclusion

Long-range capacitive sensors need accurate measurements of small capacitance variations, typically below 0.01%. To achieve this, the front-ends of the sensors should effectively reject the noise captured by the sensor transducer and introduce low noise or errors (e.g., discretization errors).

We proposed a differential analog front-end that measures the variations of the sensor capacitance by means of the phase shifts introduced onto a carrier frequency by the change of capacitance reactance. The experimental measurements using the front-end confirmed the mathematical predictions in terms of sensitivity and noise rejection, and demonstrated very good stability for the practical purpose of indoor human localization.

Acknowledgment

The authors would like to thank Osama Bin Tariq, Zohaib Aziz Mehtar and Abubakar Siddique Muqaddas, who helped during the execution of the experiments.

References

[1] T. Grosse-Puppendahl et al., “Finding Common Ground: A Survey of Capacitive Sensing in Human-Computer Interaction”, Proceedings of the SIGCHI Conference on Human Factors in Computing Systems (CHI’17). ACM, 2017.

[2] Y. Zheng et al., “Travi-navi: Self-deployable indoor navigation system”, Proceedings of the 20th annual international conference on Mobile computing and networking. ACM, 2014.

[3] G. Lu et al., “Where am i in the dark: Exploring active transfer learning on the use of indoor localization based on thermal imaging”, Neurocomputing 173 (2016).

[4] L. Mainetti, P. Luigi and S. Ilaria, “A survey on indoor positioning systems”, 22nd IEEE International Conference on Software, Telecommunications and Computer Networks (SoftCOM), 2014.

[5] B. Smagowska et al., “Effects of ultrasonic noise on the human bodya bibliographic review”, International Journal of Occupational Safety and Ergonomics, volume 19, number 2, pp. 195–202, 2013.

[6] D. Yang, W. Sheng and R. Zeng, “Indoor human localization using PIR sensors and accessibility map”, IEEE International Conference on Cyber Technology in Automation, Control, and Intelligent Systems (CYBER), 2015, pp. 577–581, 2015.

[7] S. Narayana et al., “PIR sensors: Characterization and novel localization technique”, Proceedings of the 14th International Conference on Information Processing in Sensor Networks, pp. 142–153, 2015.

[8] C. Yang and H. R. Shao, “WiFi-based indoor positioning”, IEEE Communications Magazine, volume 53, number 3, pp. 150–157, 2015.

[9] N. Fallah et al., “Indoor human navigation systems: A survey”, Interacting with Computers, 2013.

[10] A. Athalye et al., “Novel semi-passive RFID system for indoor localization”, IEEE Sensors Journal, volume 13, number 2, pp. 528–537, 2013.

[11] A. R. Akhmareh et al., “A Tagless Indoor Localization System Based on Capacitive Sensing Technology”, Sensors, volume 16, number 9, 2016.

[12] A. Arshad et al., “An activity monitoring system for senior citizens living independently using capacitive sensing technique”, Instrumentation and Measurement Technology Conference Proceedings (I2MTC), 2016 IEEE International, pp. 1–6, 2016.

[13] A. Braun et al., “Capacitive proximity sensing in smart environments”, Journal of Ambient Intelligence and Smart Environments, volume 7, number 4, pp. 483–510, 2015.

[14] D. Wang, “Basics of capacitive sensing and applications”, Application Report: SNOA927. Dallas, Texas, UAS: Texas Instruments, 2014.

[15] J. Iqbal, A. Arif, O. B. Tariq, M. T. Lazarescu and L. Lavagno, “A contactless sensor for human body identification using RF absorption signatures”, Sensors Applications Symposium (SAS), 2017 IEEE, pp. 1–6, 2017.